Phase Behavior of Symmetric Sulfonated Block Copolymers

Moon Jeong Park[†,‡] and Nitash P. Balsara*[,†,‡,§]

Department of Chemical Engineering, University of California, Berkeley, California 94720, and Materials Sciences Division and Environmental Energy Technologies Division, Lawrence Berkeley National Laboratory, University of California, Berkeley, California 94720

Received December 7, 2007; Revised Manuscript Received February 13, 2008

ABSTRACT: Phase behavior of poly(styrenesulfonate-methylbutylene) (PSS-PMB) block copolymers was studied by varying molecular weight, sulfonation level, and temperature. Molecular weights of the copolymers range from 2.9 to 117 kg/mol. Ordered lamellar, gyroid, hexagonally perforated lamellae, and hexagonally packed cylinder phases were observed in spite of the fact that the copolymers are nearly symmetric with PSS volume fractions between 0.45 and 0.50. The wide variety of morphologies seen in our copolymers is inconsistent with current theories on block copolymer phase behavior such as self-consistent field theory. Low molecular weight PSS-PMB copolymers (<6.2 kg/mol) show order−order and order–disorder phase transitions as a function of temperature. In contrast, the phase behavior of high molecular weight PSS-PMB copolymers (>7.7 kg/mol) is independent of temperature. Due to the large value of Flory–Huggins interaction parameter, χ, between the sulfonated and non-sulfonated blocks, PSS-PMB copolymers with PSS and PMB molecular weights of 1.8 and 1.4 kg/mol, respectively, show the presence of an ordered gyroid phase with a 2.5 nm diameter PSS network. A variety of methods are used to estimate χ between PSS and PMB chains as a function of sulfonation level. Some aspects of the observed phase behavior of PSS-PMB copolymers can be rationalized using χ.

Introduction

The thermodynamics and phase behavior of block and graft copolymers have attracted considerable attention in recent years.[1–10] Most of the work in this field is restricted to polymers that comprise uncharged monomers such as polystyrene (PS), polyisoprene (PI), polyethylene (PE), etc. We refer to such systems as conventional block copolymers. Theories such as the random phase approximation,[1] the Flory–Huggins theory,[2,3] and self-consistent field theory[4] have been successfully used to describe the thermodynamics and phase behavior of these systems. In fact, it is believed that the phase behavior of all conventional block copolymers can be mapped on to a universal phase diagram of the type given in ref 6.

Conventional block copolymers are important items of commerce due to their use in large volume applications such as thermoplastic elastomers and pressure sensitive adhesives. While these applications are enabled due to the ability of block copolymers to self-assemble into distinct microphases, what matters most is the viscoelastic properties of the materials while they are processed and in the final state. The microscopic structure (e.g., size and shape of microphases) within these materials is only important insofar as its effect on macroscopic mechanical properties.

More recent work[11–16] is concerned with block copolymers containing charged species either dissolved in one of the blocks such as polyethylene oxide or attached to the main chain as is the case in polystyrenesulfonate. While this class of materials has not yet found widespread use, they have the potential to serve as electrolytes for the next generation of batteries and fuel cells. The ability of block copolymers to function effectively in these applications depends entirely on the nature of the microscopic structure. For example, discrete domains of ion-conducting phases are entirely inappropriate for such applications.

* Corresponding author.
† Department of Chemical Engineering, University of California.
‡ Materials Sciences Division, Lawrence Berkeley National Laboratory.
§ Environmental Energy Technologies Division, Lawrence Berkeley National Laboratory.

The purpose of this work is to present experimental data on the thermodynamics and phase behavior of poly(styrene-sulfonate-*block*-methybutylene) (PSS-PMB) copolymers. In low dielectic media such as PS and PMB, one expects the ionic species to exist as tightly bound ion pairs. It is usually assumed that such ion pairs are not very different from uncharged molecules.[17] Based on prior work, we thus do not expect the sulfonation of the PS block to lead to behaviors that are radically different from that observed in conventional PS-PMB block copolymers.[18,19] This is consistent with the limited data obtained thus far on charge-containing block copolymers.[12,20–22]

The work presented in this paper demonstrates the existence of classical block copolymer morphologies of lamellae (LAM), gyroid, hexagonally perforated lamellae (HPL), and hexagonally packed cylinders (HEX) as the molecular weight, temperature, and sulfonation level (SL) are varied. What is surprising is that all of these morphologies are obtained in nearly symmetric block copolymers wherein the volume fraction of the PSS phase lies between 0.45 and 0.5. In this range of compositions, only LAM phases are seen in conventional block copolymers. It is clear that the introduction of sulfonic acid groups in one of the blocks results in radically different phase behavior.

Our low molecular weight PSS-PMB samples exhibit classical order–disorder phase transitions, where order is lost upon heating. We also find that increasing the SL in a given PSS-PMB copolymer stabilizes the ordered phase. This conclusion is different from the only previous report on the phase behavior of PSS-containing block copolymers[12,20–22] where it was reported that the introduction of ionic groups resulted in disorder.

Experimental Section[60]

Materials. PS-PI block copolymers were synthesized and characterized using methods described in ref 23. Molecular weights of the copolymers ranged from 2.8 to 103 kg/mol. All polymers contain 48 ± 1 wt % PS with polydispersity indices less than 1.03. Selective hydrogenation of the PI block was conducted in the presence of a homogeneous Ni−Al catalyst with cyclohexane as the solvent, using a 2 L Parr batch reactor at 83 °C and 420 psi, following procedures given in ref 24. The Ni−Al catalyst was

10.1021/ma702733f CCC: $40.75
Published on Web 04/25/2008

prepared by combining 50 mL of 0.1 M nickel 2-ethylhexanoate in cyclohexane (Aldrich) with 20 mL of 1.0 M triethylaluminium in heptanes (Aldrich). After the reaction, the catalyst was removed by vigorously stirring the reaction mixture with 10% aqueous citric acid. The hydrogenation reaction was repeated about 4 times until diene groups were not detected in the ^{1}H nuclear magnetic resonance (NMR) spectra of the polymer. The NMR spectra also confirmed that the styrene units were not saturated, and gel permeation chromatography (GPC) confirmed that there was no chain degradation. The hydrogenated block copolymers are referred to as PS-PMB copolymers. The PS blocks of the PS-PMB copolymers were then partially sulfonated using procedures described in ref 25. 40 mL of 1,2-dichloroethane and 1 g of PS-PMB were added to a 100 mL three-neck flask equipped with a funnel and condenser. The mixture was heated to 40 °C under a N_2 blanket and stirred until the copolymer was completely dissolved. Acetic sulfate was prepared by injecting 1.8 mL of acetic anhydride and 5.4 mL of dichloroethane into a sealed N_2-purged round-bottomed flask. The solution was cooled to 0 °C and 0.5 mL of 96% sulfuric acid was injected into the flask. The acetic sulfate was immediately transferred to the flask containing the PS-PMB/dichloroethane mixture at 40 °C using a funnel. The reaction was terminated with 20 mL of 2-propanol. Samples with different SL were prepared by controlling reaction time. The polymer in the reaction mixture was purified by dialysis against pure water using a cellulose dialysis membrane with a 3.5 kg/mol molecular weight cutoff (VWR) for 10 days. In the case of PSS-PMB copolymers with molecular weights in the vicinity of the dialysis membrane cutoff, the time required for this step is crucial as waiting too long results in loss of the polymer sample while waiting for only a short period of time results in acid contamination of the polymer. NMR measurements were used to determine the acid concentration in the polymer as it was dialyzed. The polymer was then recovered by vacuum drying at 60 °C for 7 days.

Our synthetic procedure is summarized in Figure 1. The sulfonated block copolymers are referred to as PSS-PMB copolymers.

^{1}H Nuclear Magnetic Resonance (NMR). All of the NMR experiments were conducted on a 500 MHz Bruker AV500 spectrometer. Typical ^{1}H NMR spectra (in acetone-d_6) obtained from our samples are shown in Figure 1 where spectral peak assignments obtained from P9 are shown. Non-sulfonated styrene units exhibit peaks at 6.4–6.8 ppm (a) and 6.9–7.3 ppm (b). Upon sulfonation, a new peak is obtained at 7.4–7.8 ppm (c). The SL of PSS-PMB copolymers was calculated by the equation:

$$\mathrm{SL} = \left(\frac{\text{moles of styrenesulfonate}}{\text{moles of styrene} + \text{moles of styrenesulfonate}}\right) = \frac{\text{integrals of peak c/2}}{\text{integrals of (peak c/2} + \text{peak b/3)}} \quad (1)$$

Small-Angle X-ray Scattering (SAXS). One mm thick PSS-PMB samples were prepared by solvent casting using THF as a solvent under nitrogen blanket for 2 days followed by vacuum drying at 50 °C for 10 days. Synchrotron SAXS measurements on these samples were performed using the 15-ID-D beam line at the Advanced Photon Source (APS). Sample temperature was controlled within ±0.2 °C using a sample stage provided by the APS. Samples were equilibrated for at least 15 min before measurement. The wavelength (λ) of the incident X-ray beam was 0.15 nm ($\Delta\lambda/\lambda = 10^{-4}$), and sample-to-detector distance of 2.0 m was used, yielding scattering wave vector q ($q = 4\pi \sin(\theta/2)/\lambda$, where θ is the scattering angle) in the range 0.1–2.5 nm^{-1}. The resulting two-dimensional scattering data were averaged azimuthally to obtain intensity versus q. The scattering data were corrected for the CCD dark current and the scattering from air and Kapton windows.

Transmission Electron Microscopy (TEM). The PSS-PMB samples prepared by the same method used to prepare the SAXS samples were cryo-microtomed at −100 °C to obtain thin sections with thicknesses in the 50–80 nm range using an RMC Boeckeler PT XL Ultramicrotome. The electron contrast in the dry polymer samples was enhanced by exposure to ruthenium tetroxide (RuO_4) vapor for 50 min. Imaging of stained samples was performed with a Zeiss LIBRA 200FE microscope operating at 200 kV equipped with a cold stage (−160 °C) and an Omega energy filter. To prevent beam damage, the polymer sections evacuated at 10^{-5} Pa were placed on the cold stage before they were exposed to the electron beam. Images were recorded on a Gatan 2048 × 2048 pixel CCD camera. (Gatan Inc., Pleasanton, CA). All data sets were acquired using Digital Micrograph (Gatan, Inc.) software. The TEM images thus enable quantification of the room temperature morphology of our PSS-PMB copolymers.

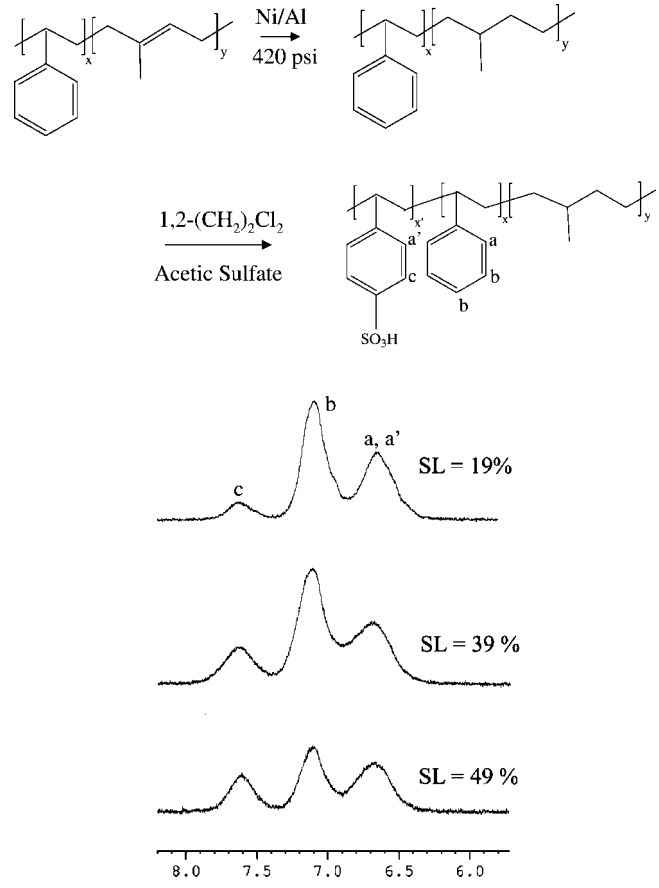

Figure 1. Synthesis of PSS-PMB block copolymers and representative ^{1}H NMR spectra for P9 series with different sulfonation levels.

In Situ Small-Angle Neutron Scattering (In Situ SANS). The SANS samples were prepared by solvent casting the PSS-PMB polymer from THF solutions on 1 mm quartz windows under nitrogen blanket for 2 days followed by vacuum drying at 50 °C for 10 days. The sample thickness ranged from 50 to 180 μm and a circular area with a diameter of 1.8 cm was exposed to the neutron beam. The sample thicknesses used represent a compromise between time required for equilibration with the surrounding air which decreases as the sample thickness decreases, and the measured SANS scattering signal which increases as the sample thickness increases. The samples were studied using the 30 m NG7 beamline at the National Institute of Standards and Technology (NIST) equipped with a sample holder wherein the humidity of the surrounding air and sample temperature were controlled. The uncertainties of the sample humidity and temperature for the NIST humidity sample chamber are ±1% relative humidity (RH) and ±1 °C, respectively. The λ of the incident neutron beam was 0.6 nm ($\Delta\lambda/\lambda = 0.10$), and sample-to-detector distance of 3.0 m was used. This enabled access to scattering at q values in the range 0.1–2.5 nm^{-1}.

Table 1. Materials Used in Present Study

sample code[a]	SL (mol%)	mol wt (PSS-PMB) (kg/mol)	morphology at 25 °C	ϕ_{PSS}[b]
P1(0)	0	1.4–1.4	disorder	0.459
P1(18)	17.8	1.5–1.4	disorder	0.472
P1(31)	30.7	1.7–1.4	disorder	0.480
P1(32)	32.1	1.8–1.4	gyroid	0.481
P1(44)	44.0	2.0–1.4	gyroid	0.489
P3(0)	0	2.5–2.6	disorder	0.455
P3(11)	11.2	2.8–2.6	disorder	0.458
P3(19)	18.9	3.0–2.6	LAM	0.464
P3(21)	20.9	3.1–2.6	LAM	0.465
P3(32)	31.9	3.5–2.6	HPL	0.473
P3(44)	44.3	3.6–2.6	HPL	0.480
P4(0)	0	3.5–3.7	disorder	0.445
P4(17)	17.4	4.0–3.7	gyroid	0.457
P4(22)	22.1	4.1–3.7	gyroid	0.461
P4(24)	24.4	4.3–3.7	LAM	0.462
P4(38)	38.3	4.6–3.7	HPL	0.471
P4(45)	44.7	4.8–3.7	HPL	0.476
P5(0)	0	4.8–4.6	LAM	0.472
P5(7)	6.7	5.1–4.6	LAM	0.477
P5(21)	20.7	5.6–4.6	LAM+HPL	0.485
P5(40)	39.6	6.4–4.6	HPL	0.498
P5(47)	47	6.9–4.6	HEX	0.503
P5(53)	52.9	7.1–4.6	HEX	0.507
P9(0)	0	9.1–8.7	LAM	0.473
P9(19)	18.5	10.6–8.7	LAM+HPL	0.484
P9(25)	25.2	11.3–8.7	HEX	0.491
P9(39)	38.7	12.1–8.7	HEX	0.499
P9(49)	48.6	12.8–8.7	HEX	0.506
P9(53)	53.3	13.2–8.7	HEX	0.509
P21(0)	0	20.7–21.3	LAM	0.453
P21(5)	5.1	22.3–21.3	LAM	0.458

[a] Samples are labeled according to the nominal molecular weight of the nonsulfonated PS block and the sulfonation level (SL). Sample P1(32), for example, is the PSS-PMB block copolymer with a 1.4 kg/mol PS block with SL = 32%. [b] The estimated error in the determination of ϕ_{PSS} is 0.000.

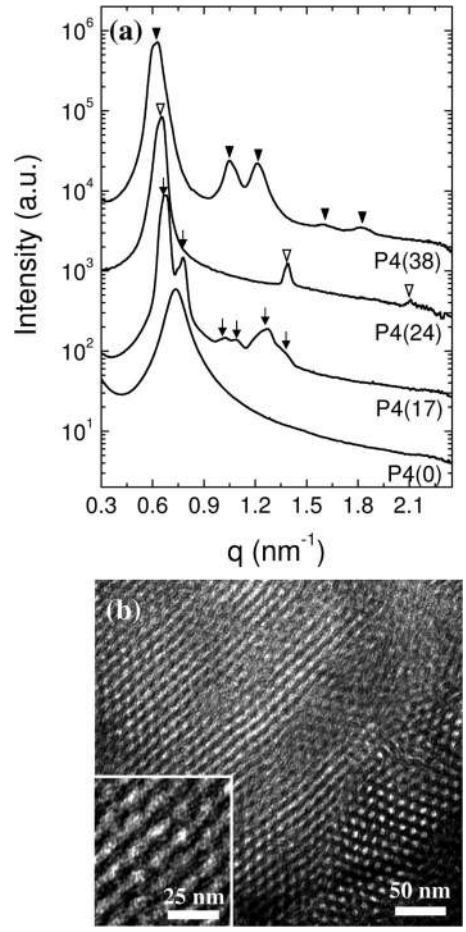

Figure 2. (a) SAXS profiles of P4 samples as a function of sulfonation level (SL) at 25 °C. The arrows (↓) of P4(17), the inverted open triangles (▽) of P4(24), and the inverted filled triangles (▼) of P4(38) indicate Bragg peaks at $\sqrt{6}q^*$, $\sqrt{8}q^*$, $\sqrt{14}q^*$, $\sqrt{16}q^*$, $\sqrt{20}q^*$, $\sqrt{24}q^*$, at q^*, $2q^*$, $3q^*$, and at q^*, $\sqrt{3}q^*$, $\sqrt{4}q^*$, $\sqrt{7}q^*$, and $\sqrt{9}q^*$, respectively. The scattering profiles of P4(17), P4(24), and P4(38) are offset vertically by factors of 10, 10^2, and 10^3, respectively, for clarity. (b) Cross-sectional TEM image of P4(38) showing hexagonally perforated lamellar phases. The image obtained with higher magnification is shown in (b) as inset box to verify the presence of perforated layers. PSS domain was darkened by RuO_4 staining.

Phase Behavior of PSS-PMB

The characteristics of PSS-PMB copolymers used in this study are listed in Table 1. Samples are labeled according to the nominal molecular weight of the nonsulfonated PS block and the SL value of the copolymer. Sample P1(32), for example, is the PSS-PMB block copolymer with a 1.4 kg/mol PS block with SL = 32%. The volume fraction of PSS, ϕ_{PSS}, was calculated using pure component densities of polystyrene, ρ_{PS} = 1.05 g/cm^3, fully sulfonated polystyrene, ρ_{SPS} = 1.44 g/cm^3, and poly(methylbutylene) ρ_{PMB} = 0.86 g/cm^3, ignoring volume changes of mixing.[26,27]

We begin by describing the phase behavior in the vicinity of room temperature. The SAXS experiments were performed at 25 °C while the TEM samples were prepared at room temperature which was 22 °C, on average. In all cases, the morphology obtained by SAXS at 25 °C was confirmed by TEM. For brevity, we only discuss representative data obtained from a subset of the samples listed in Table 1. Figure 2 shows SAXS profiles obtained from the P4 series at 25 °C. The SAXS profile of the unsulfonated P4(0) sample contains one broad peak characteristic of disordered concentration fluctuations.[1] The data in Figure 2a indicate that the sulfonation of the PS block at 25 °C first leads to a disorder-to-gyroid transition followed by a series of order-order transitions. The data from P4(17) show Bragg peaks at $\sqrt{6}q^*$, $\sqrt{8}q^*$, $\sqrt{14}q^*$, $\sqrt{16}q^*$, $\sqrt{20}q^*$, $\sqrt{24}q^*$, where $q^* = 2\pi/d_{211}$ with d_{211} = 9.05 nm, characteristic of the gyroid phase with $Ia\bar{3}d$ space-group symmetry.[28,29] The Miller indices corresponding to the observed Bragg peaks are (211), (220), (321), (400), (420), and (422).[30] Qualitatively different SAXS peaks are observed in P4(24) where the presence of $1q^*$:$2q^*$:$3q^*$ Bragg peaks with $q^* = 2\pi/d_{100}$, where d_{100} = 9.88 nm, as shown by inverted open triangles (▽), indicate the formation of a LAM morphology. A further increase in the SL reveals a series of Bragg peaks (▼) at q^*, $\sqrt{3}q^*$, $\sqrt{4}q^*$, $\sqrt{7}q^*$, and $\sqrt{9}q^*$, where $q^* = 2\pi/d_{100}$ with d_{100} = 10.1 nm indicative of a HPL morphology.[31] The relative locations (characteristic q) of the higher order SAXS peaks of the HPL phase depend on whether the perforations are arranged on a trigonal (ABC stacking) or hexagonal (AB stacking) lattice.[31] For the case of AB stacking, the relative locations of the higher order SAXS peaks of the HPL phase are identical to those of the HEX phase. The SAXS data from P4(38) indicate the presence of AB stacking. In such cases TEM must be used to distinguish between HPL and HEX phases. The TEM micrograph of P4(38), shown in Figure 2b, suggests the presence of lamellae with perforations (edge view) and the hexagonal arrangement of the perforations (top view). We examined several P4(38) samples by TEM and were unable to find the (100) plane of the HEX phase. We thus conclude that the structure of P4(38) at room temperature is HPL.

Note that the gyroid structure with SL = 17% has PSS minor domains while the HPL phase with SL = 38% possesses major PSS domains. Since the change in ϕ_{PSS} for this phase inversion, calculated from densities of each component, is insignificant

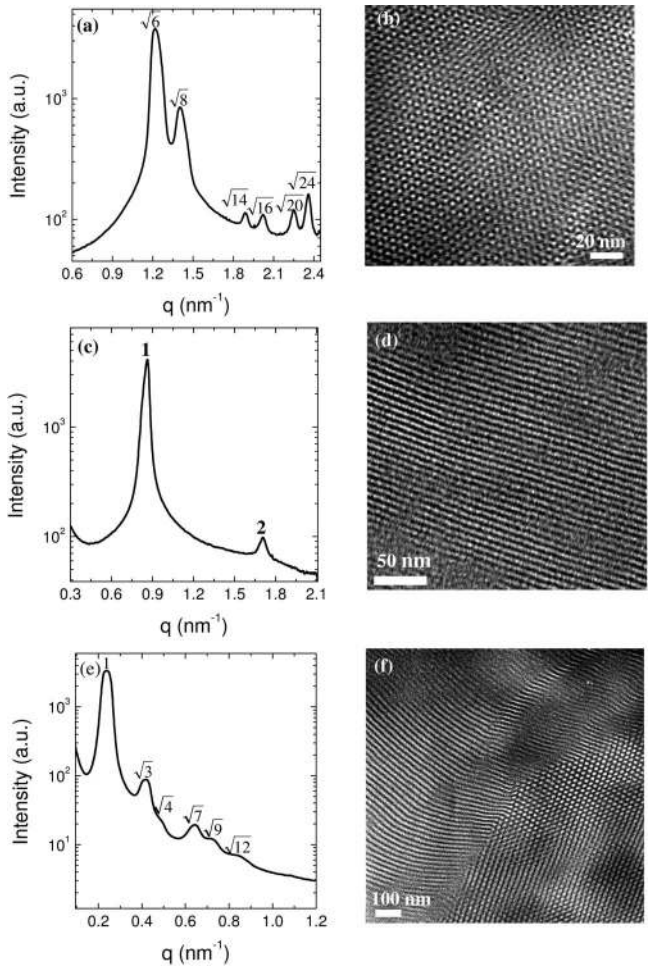

Figure 3. SAXS profiles and cross-sectional TEM images of P1(32) (a, b), P3(21) (c, d), and P9(39) (e, f). PSS domain was darkened by RuO_4 staining.

(0.461 to 0.471), it is clear that the introduction of sulfonic acid groups in PS blocks results in radically different phase behavior from uncharged block copolymers. It should be also noted here that due to the coarse sulfonation steps in our PSS-PMB copolymers, other phases may exist at intermediate sulfonation levels.

Similar phase transitions of disorder to gyroid to HPL to LAM, with decreasing in temperature have been reported before in PS-PI with PI volume fraction = 0.65,[32] in poly(ethylene oxide)-*b*-poly(ethylethylene) (PEO-PEE) with PEO volume fraction = 0.70,[33] and in poly(methylbutylene)-*b*-poly(dimethylsiloxane) (PMB-PDMS) with PMB volume fraction = 0.64.[34] In conventional polymers, this sequence is a consequence of increasing segregation strength, i.e., increasing χN, where χ is the Flory–Huggins interaction parameter and N is number of monomers per chain.[1,35,36] The fact that we observe the same sequence as a function of increasing ion content suggests that the incorporation of ionic groups leads to increased segregation of the blocks. However, direct comparisons between conventional block copolymer and our sulfonated block copolymers may not be appropriate due to the presence of ionic groups.

The room temperature phase behavior of PSS-PMB is a sensitive function of molecular weight of copolymers. The SAXS profile of P1(32) shown in Figure 3a is very similar to that shown in Figure 2a and indicates the presence of a gyroid structure. This gyroid morphology was also clearly observed by TEM. In Figure 3b we show the wagon-wheel structure obtained from P1(32) after the PSS phase is stained with RuO_4. The domain spacing of the P1(32) gyroid, obtained from both SAXS and TEM, is about 5 nm, implying that the diameter of the PSS network is 2.5 nm. To our knowledge, the ordered phase in P1(32) is the smallest ordered structure obtained by self-assembly in block copolymers. This indicates that χ between PSS and PMB is very large in spite of the fact that only 32% of the styrene groups were sulfonated. P1 samples were disordered when the SL was below 32% (e.g., 31% and 18%).

The ordered phase formed by symmetric uncharged block copolymers with minor component volume fractions in the 0.45 to 0.50 range is LAM. We thus expect all of the PSS-PMB copolymers to exhibit a LAM phase at low SLs. The P3, P4, and P5 series show a LAM phase when SL is around 22%. P1 is disordered in this regime. Data shown in Figure 3c,d, where SAXS and TEM results from P3(21) indicate a LAM phase with $d = 7.5$ nm, are examples of such data. With increase in SL up to 47%, HPL morphology is obtained for the P3, P4, and P5 series. In contrast, for the case of P9 samples (high molecular weight samples), HEX phase was obtained at SL values greater than 25%. The SAXS profiles of P9(39) shown in Figure 3e contains peaks at q^*, $\sqrt{3}q^*$, $\sqrt{4}q^*$, $\sqrt{7}q^*$, $\sqrt{9}q^*$, and $\sqrt{12}q^*$, where $q^* = 2\pi/d_{100}$. This sequence of peaks is identical to that obtained from P4(38) shown in Figure 2a. However, the TEM data from P4(38) and P9(39) are entirely different. The TEM data of P9(39) shown in Figure 3f confirms the HEX morphology of the sample viewed along [100] (top area) and [001] (bottom area) direction, respectively. Numerous samples of P9(25), P9(39), P9(49), and P9(53) were examined by TEM. None of them showed any evidence of perforated structures like those seen in Figure 2b. This implies that the stability window of the HPL morphology becomes narrower and eventually disappears with increase in molecular weight.

We now discuss the temperature dependence of the phase behavior of PSS-PMB copolymers. In all cases, we found that the SAXS intensity decreases with increasing temperature indicating typical upper critical solution temperature (UCST) behavior. This was true irrespective of the SL of the copolymer or molecular weight. Low molecular weight samples exhibited order-to-disorder transitions (ODT) upon heating. Examples of such data are shown in Figures 4a and 4b, where SAXS profiles of P1(32) and P3(19), respectively, are shown as a function of temperature. The higher order peaks of P1(32) and P3(19) obtained at low temperatures, indicative of the presence of ordered phases, disappear at a temperature between 53 and 55 °C (Figure 4a) and between 72 and 74 °C (Figure 4b), respectively. We conclude that the ODT temperature, T_{ODT}, of P1(32), is 54 ± 1 °C and T_{ODT} of P3(19) is 73 ± 1 °C.

The formation of the HPL phase in PSS-PMB is reversible. This is illustrated in Figure 5 where SAXS data obtained from P3(32) are shown. Samples were equilibrated for 15 min at each temperature before measurement. At 30 °C, after solvent casting, P3(32) shows classical signatures of an HPL phase. At 60 °C, we find that the scattering peaks corresponding to the HPL phase (identified in Figure 5 by ▽) persist but new peaks corresponding to a LAM phase emerge (identified by in Figure 5 by ↓). At 90 °C, the HPL phase is no longer evident and only the LAM phase is seen. Cooling the sample to 60 °C does not lead to a change in structure and only the LAM phase is evident. Further cooling to 30 °C, however, leads to the disappearance of the LAM peaks and the reemergence of the HPL peaks (Figure 5). The primary and higher order scattering peaks are not as sharp in the cooling run as they were in the heating run. The 30 °C heating run data were obtained from a solvent-cast sample wherein the presence of the solvent during ordering increases molecular mobility which in turn reduces defect density of the HPL phase and facilitates structure determination. In contrast,

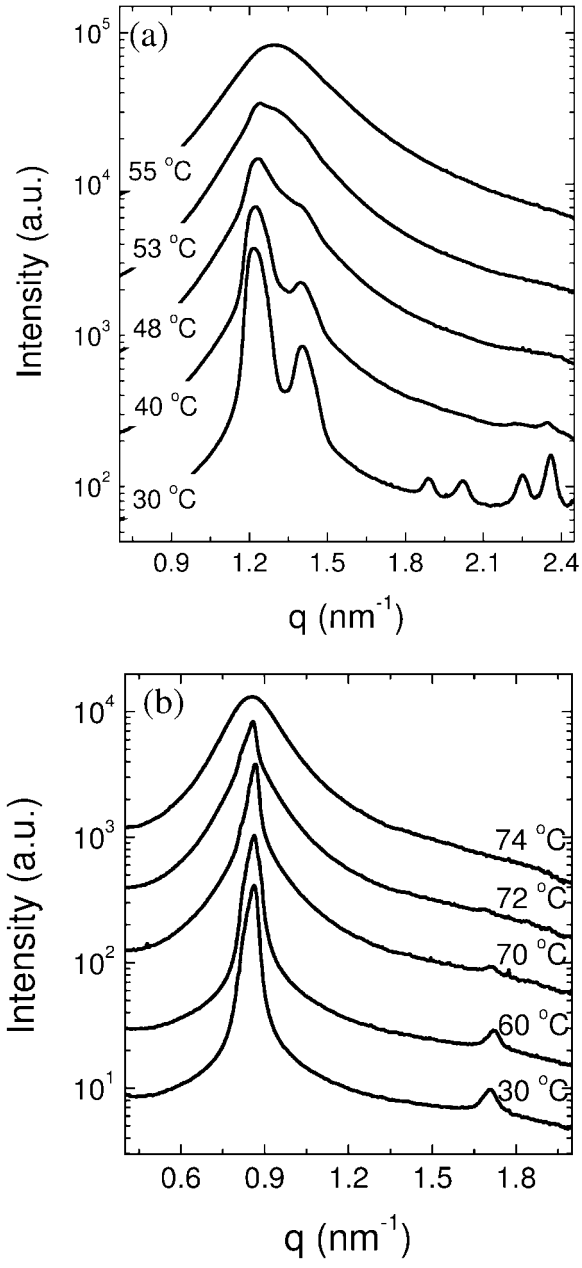

Figure 4. SAXS profiles of (a) P1(32) and (b) P3(19) as a function of temperature, indicating $T_{ODT} = 54 \pm 1$ °C (a) and $T_{ODT} = 73 \pm 1$ °C (b), respectively. The scattering profiles are offset vertically by factors of 3.3, 3.3^2, 3.3^3, and 3.3^4, for clarity.

the HPL phase formed after cooling the LAM phase is formed in the melt and defect annihilation in these systems is expected to be much slower than that in the presence of the solvent. The data in Figure 5 clearly demonstrate that the HPL-to-LAM phase transition is reversible. The q^* value changes by about 6% (LAM spacing is larger than HPL spacing) for the case of P3(32). This is in good agreement with previous results on conventional block copolymers which show an increase in q^* between 5 and 9%.[19,37] We can assert that the HPL to LAM transition occurs between 30 and 90 °C, but the exact temperature at which this phase transition occurs cannot be determined from our work thus far. The reversible formation of the HPL phase in PSS-PMB is similar to that obtained in conventional block copolymers.[19,37]

Higher molecular weight PSS-PMBs show windows where coexistence of LAM and HPL phases are seen in the 21% < SL < 40% window for P5 series and the SL < 25% window for P9 series. Typical data obtained from such systems are shown in Figure 6 where SAXS data from P9(19) at 25 °C are shown. Peaks at q^*, $\sqrt{3}q^*$, $\sqrt{4}q^*$, $\sqrt{7}q^*$, and $\sqrt{9}q^*$ (indicated by ▼) representing the HPL structure are seen to coexist with the $1q^*$, $2q^*$, and $3q^*$ (indicated by ▽) representing the LAM. The domain spacing of the HPL phase is 15% larger than that of LAM phase. Such a large difference has not been noted in

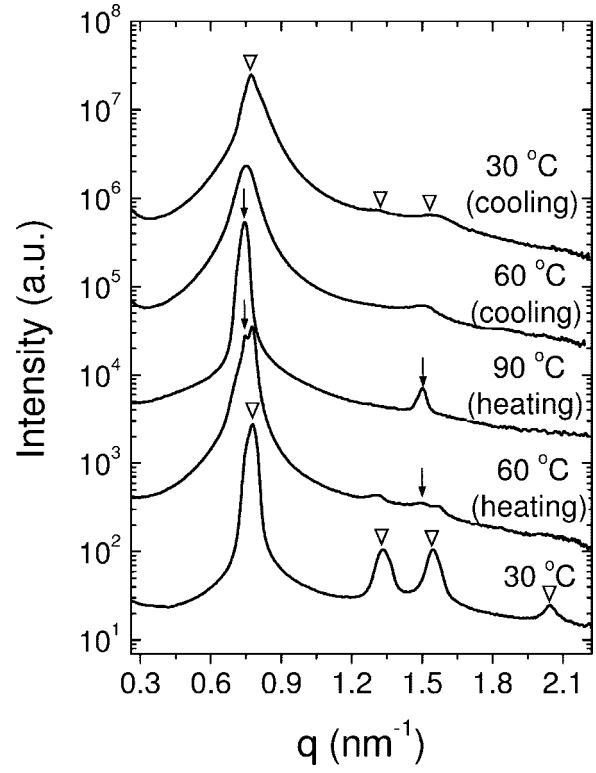

Figure 5. SAXS profiles of P3(32) during heating and cooling scans showing the thermally reversible phase transition from HPL-to-LAM. The arrows (↓) and the inverted open triangles (▽) indicate Bragg peaks of LAM and those of HPL, respectively. The coexistence of HPL and LAM is seen at 60 °C (heating). The scattering profiles are offset vertically by factors of 20, 20^2, 20^3, and 20^4, for clarity.

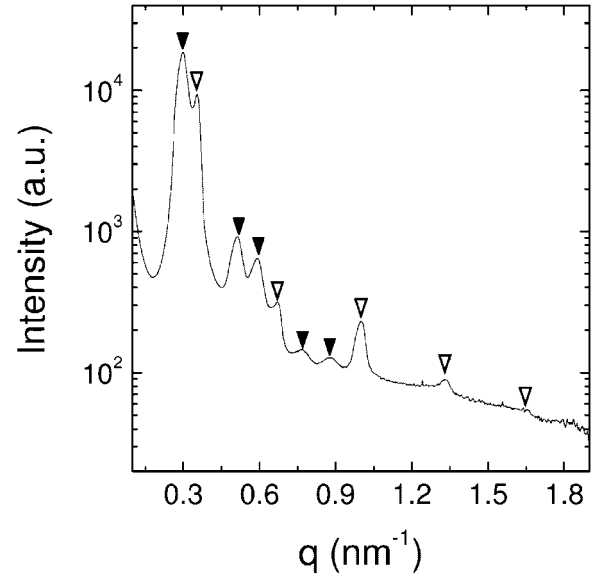

Figure 6. SAXS profiles of P9(19) at 25 °C showing the coexistence of HPL and LAM structures. The inverted filled triangles (▼) at $1q^*$, $\sqrt{3}q^*$, $\sqrt{4}q^*$, $\sqrt{7}q^*$, and $\sqrt{9}q$ and the inverted open triangles (▽) at $1q^*$, $2q^*$, $3q^*$, $4q^*$, $5q^*$ represent HPL and LAM, respectively.

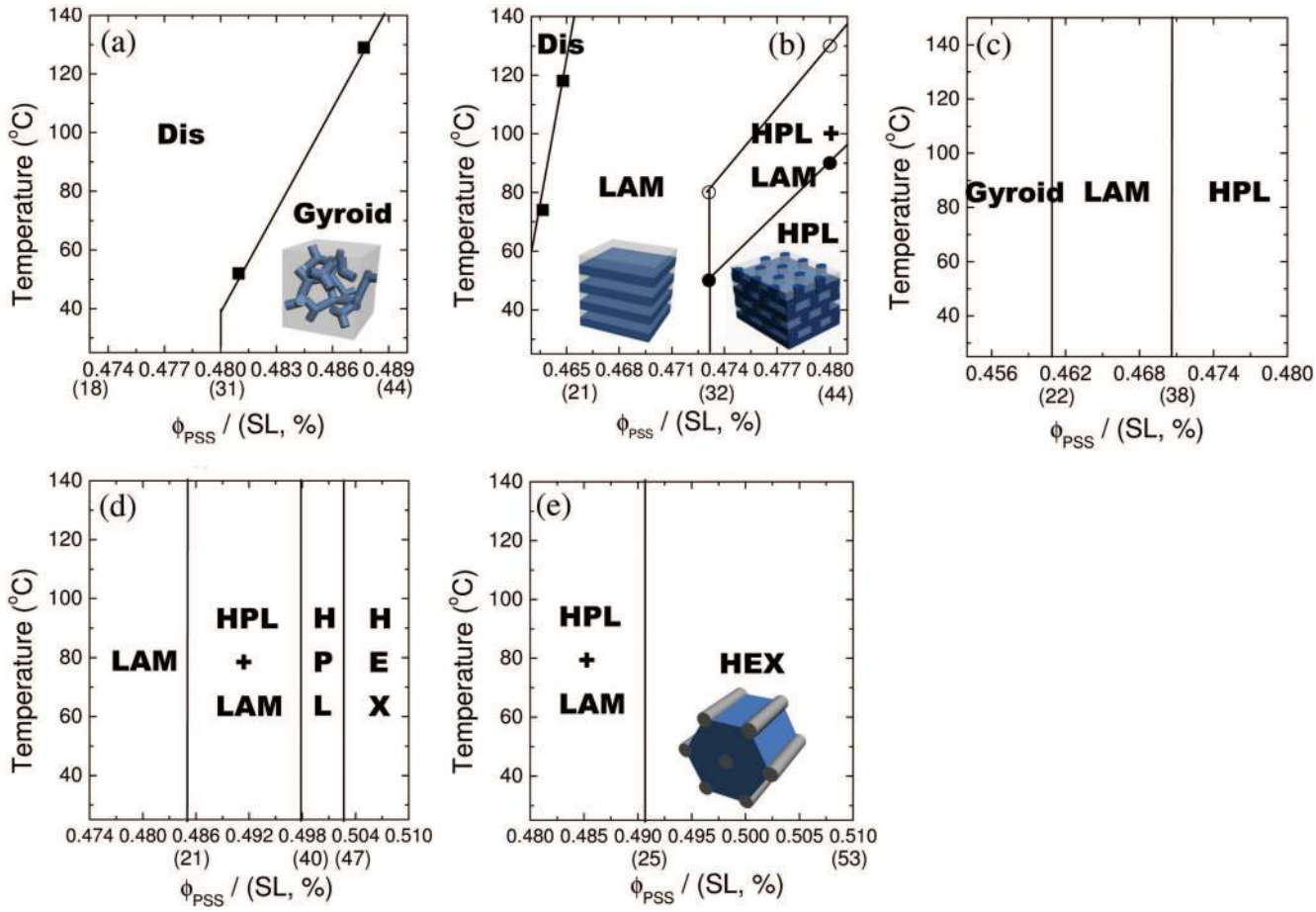

Figure 7. Phase diagrams of PSS-PMBs: (a) P1 series ($N = 54$), (b) P3 series ($N = 99$), (c) P4 series ($N = 141$), (d) P5 series ($N = 184$), and (e) P9 series ($N = 347$), respectively. The volume fraction of PSS block (ϕ_{PSS}) changes due to changes in the sulfonation level as indicated below the x-axis.

conventional block copolymers exhibiting an HPL-to-LAM transition. The LAM+HPL coexistence is seen from room temperature up to 150 °C. This suggests that the LAM+HPL coexistence may be an equilibrium property of PSS-PMB copolymers. From a theoretical point of view, coexisting phases cannot exist at equilibrium in perfectly monodisperse conventional block copolymers.[1,38] This is in good agreement with carefully conducted experiments on anionically synthesized block copolymers.[3,32,39–41] There are, however, some reports of coexisting phases in conventional block copolymers.[42–46] This kind of behavior must arise due to polydispersity in chain length and/or composition. In PSS-PMB copolymers there is an additional source of polydispersity—the location and concentration of the sulfonic acid groups. We expect a distribution of concentration of sulfonic acid groups per chain in our sample due to the randomness of the sulfonation reaction. Chains with slightly different SLs may behave differently due the extremely large χ parameter between sulfonated and nonsulfonated monomers. Thus, it is conceivable that the LAM regions of the coexisting phase contain chains with lower SLs than those in the HPL regions.

For a random process, we expect the width of the distribution to decrease as $1/N_s^{0.5}$, where N_s is the average number of sulfonic acid groups on the chain. Thus, we expect the SL distribution functions to be wider in the case of the lower molecular weight samples. If the observed LAM+HPL coexistence was simply due to polydispersity, then we would have expected to see it in the low molecular weight samples. On the contrary, we have observed coexistence in only P5 and P9 samples, i.e., samples with the highest molecular weight. Furthermore, the coexistence is seen at intermediate SLs (between 21 and 40 for P5 samples). It is evident that an understanding of the origin of the LAM+HPL coexistence will require analysis that is beyond the scope of the present paper.

The methodology outlined above was used to study the properties of all of the PSS-PMB samples listed in Table 1. The phase diagrams for symmetric PSS-PMB copolymers of different molecular weights as a function of the volume fraction of the PSS block, ϕ_{PSS} (SL is also indicated below the x-axis) and T are shown in Figure 7. Sulfonation results in modest changes in ϕ_{PSS} from 0.445 to 0.509. In spite of the limited range of ϕ_{PSS} values, a rich variety of morphologies are obtained.

P1 samples form a gyroid phase when $0.480 < \phi_{PSS} < 0.490$ (Figure 7a) with accessible order–disorder transition temperatures. A large portion of the T-ϕ_{PSS} window studied is taken up by the disordered state. Neglecting the small change in N upon sulfonation, and using the formulas applicable at the order–disorder transitions for symmetric copolymers[1,2]

$$\chi = \frac{10.5}{N}; \quad \text{Leibler} \tag{2}$$

$$\chi = \frac{10.495 + 41.0N^{-1/3}}{N}; \quad \text{Fredrickson–Helfand (F-H)} \tag{3}$$

where $N = (v_{PSS}/v_0)N_{PSS} + (v_{PMB}/v_0)N_{PMB}$ are calculated based on a reference volume, v_0, of 0.1 nm^3, PSS segment volume, v_{PSS}, of 0.179 nm^3, and PMB segment volume, v_{PMB}, of 0.147 nm^3. The N of P1(0) and P1(18) is 54. We conclude that at the ODT (54 °C), $\chi_{PSS\text{-}PMB} = 0.194$ based on the Leibler theory[1] and $\chi_{PSS\text{-}PMB} = 0.395$ based on the F-H theory.[2,47]

P3 samples form LAM and HPL in the range $0.464 < \phi_{PSS} < 0.480$ (Figure 7b). We also found coexistence between LAM and HPL over a substantial portion of the accessible $T-\phi_{PSS}$ window in P3 samples. It is evident that the phase behavior of P3 and P1 are qualitatively different in spite of the similarity of SLs and ϕ_{PSS} values. The disordered region occupies a much smaller portion of the $T-\phi_{PSS}$ phase diagram in P3 (Figure 7b) relative to P1 (Figure 7a). The ODTs of P3(19) and P3(21) are located at 73 ± 1 °C and 119 ± 1 °C, respectively. This can be rationalized on the basis of classical block copolymer thermodynamic eqs 2 and 3; N for P3 is 99 compared to $N = 54$ for P1. Using eqs 2 and 3, we obtain $\chi_{PSS\text{-}PMB} = 0.106$ at the ODTs based on the Leibler theory and $\chi_{PSS\text{-}PMB} = 0.196$ at the ODTs based on the Fredrickson−Helfand theory. The fact that both the Leibler and Fredrickson−Helfand theories apply to block copolymers that form only lamellar phases in this range of compositions indicates that eqs 2 and 3 are only approximately valid in the case of PSS-PMB copolymers.

The phase behavior of P4, P5, and P9 are independent of temperature, as shown in Figures 7c, d, and e. In P4, the gyroid structure is obtained when $\phi_{PSS} < 0.461$, while LAM and HPL structures are seen as the SL is increased. We were unable to detect the LAM+HPL coexistence in P4 probably due to the coarse sulfonation steps that were employed to study the phase behavior. The gyroid phase is not observed in P5 and P9. Instead LAM and HPL structures are seen at low SLs, and HEX phases are seen at high SLs. The inaccessibility of the ODTs in P4, P5, and P9 can be rationalized due to the relatively large values of $N = 141$, 184, and 347, respectively, and thus the product χN is substantially larger than that needed for accessible order–disorder phase transitions.

While we have used classical block copolymer theories to rationalize some of our observations, these theories provide no basis for understanding the origin of the wide range of morphologies seen in our system. It is clear that the universal block copolymer phase diagram established in conventional block copolymers does not apply to PSS-PMB copolymers.

It is interesting to note that the results of our study are markedly different from previous studies of the morphology of sulfonated PS-based block copolymers. In the most complete study to date, SAXS and TEM data on poly(styrenesulfonate-*b*-isobutylene-*b*-styrenesulfonate) (S-SIBS, $N \approx 450$)[12,13] and poly(styrenesulfonate-*b*-[ethylene-*co*-butylene]-*b*-styrenesulfonate) (S-SEBS, $N \approx 700$)[20,22] copolymers indicated that long-range order was seen at low values of SL only. When SL was greater than 36%, long-range order was lost. Since the tendency for order formation is expected to increase with sulfonation due to increased repulsion between the blocks, the authors attributed this observation to the formation of ionic aggregates. In contrast, the PSS-PMB copolymers studied here showed well-ordered morphologies up to SL values as high as 53%. Disorder is only obtained in the low sulfonation and low molecular weight limit as expected from thermodynamic arguments. The difference between data reported in here and that reported in refs 12, 13, 20, and 22 may arise due to two differences. (1) The PDIs of pristine block copolymers before sulfonation, i.e., the SEBS and SIBS copolymers, used in refs 12, 13, 20, and 22 were 1.2 and 1.47, respectively, while that in our PS-PMB was less than 1.03. (2) The large values of N of the copolymers used in refs 12, 13, 20, and 22 may have hindered equilibration of the morphology. The use of triblock copolymers in refs 12, 13, 20, and 22 may also contribute to longer equilibration times.

We conclude this section by addressing the issue of water contamination. All of the results reported in this paper were obtained under ambient conditions, i.e., in the presence of air with nonnegligible concentrations of water vapor. Since the hygroscopic nature of PSS is well established, it is important to consider the effect of water contamination on the results described above. The relative humidity, RH, of the air in our laboratories is approximately 32%. In related but separate studies, we examined the properties of PSS-PMB membranes as a function of the humidity of the surrounding air.[48,49] In these studies, we found no change in phase behavior when the relative humidity of the air was varied from 25 to 50%, regardless of sulfonation level and copolymer molecular weight. This indicates that water contamination that was not controlled in this study has negligible effect on phase behavior of PSS-PMB copolymers in the presence of ambient air. Water uptake studies indicated that the weight fraction of water in these samples at RH = 32% ranged from 0.7 to 3.2 wt % for the range of molecular weights and sulfonation levels covered in this work.

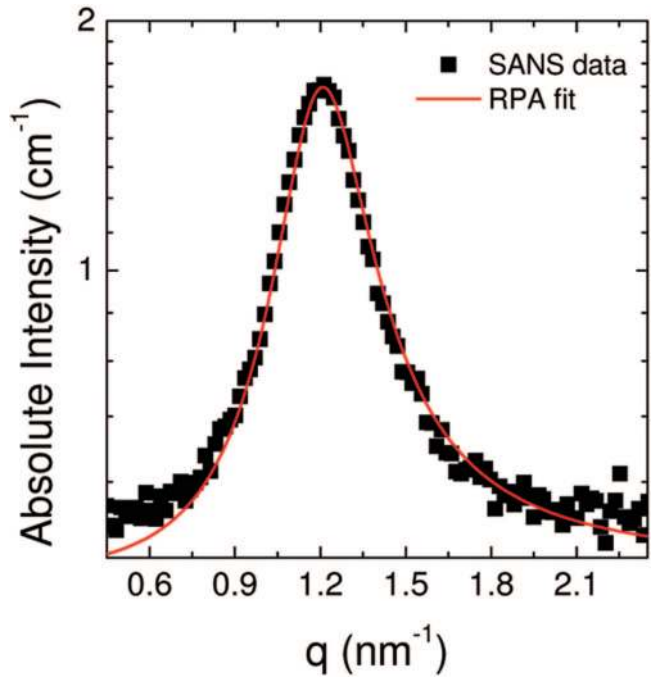

Figure 8. SANS profile from P1(31) at RH = 25% and $T = 25$ °C (symbols) and the least-squares fit using the random phase approximation with $\chi_{PSS\text{-}PMB}$ as the adjustable parameter (curve). Error bars are smaller than the symbols.

Thermodynamic Underpinnings of Phase Behavior

In our discussion of the thermodynamic interactions between PSS and PMB chains, we have treated the PSS chain as a "homopolymer". This is valid because mean-field theories are based on coarse-grained chains.[50] The parameter $\chi_{PSS\text{-}PMB}$ represents an "effective" Flory–Huggins interaction parameter between PSS and PMB chains. While we have estimated $\chi_{PSS\text{-}PMB}$ from the location of the order–disorder transitions in PSS-PMB copolymers, an alternative approach for determining $\chi_{PSS\text{-}PMB}$ is by measuring the structure factor of disordered PSS-PMB block copolymers, as has been done in numerous previous publications.[1,50–52] In Figure 8, we show the measured in situ SANS scattering profile of P1(31) at 25 °C and RH = 25% (the lower limit of NIST humidity chamber). The sample was equilibrated under these conditions for 2 h to remove the small amount of water absorbed by the sample due to extensive contact with ambient air. The water uptake of P1(31) under these conditions is less than 1%, which we consider equivalent to a completely dry sample. (Studying samples with less moisture would require entirely different instrumentation.) The predicted expression for $I(q)$ based on the random phase approximation (RPA) is[1]

$$I(q) = \left(\frac{b_1}{v_1} - \frac{b_2}{v_2}\right)^2 \left[\frac{S_{11} + S_{22} + 2S_{12}}{S_{11}S_{22} - (S_{12})^2} - \frac{2\chi_{\text{PSS-PMB}}}{v_0}\right]^{-1} \quad (4)$$

where the subscripts 1 and 2 refer to the PSS and PMB blocks, respectively, b_i and v_i are the scattering lengths and volumes, respectively, and $\chi_{\text{PSS-PMB}}$ is the effective Flory–Huggins interaction parameter[35,36] based on reference volume v_0, which we set to 0.1 nm^3. S_{ii} and S_{ij} are the ideal intrablock and interblock correlations between blocks i and j, described by the Debye and the Leibler functions, respectively. The statistical segment lengths for PS = 0.5 nm and PMB = 0.63 nm were obtained from the literature.[53] For simplicity it was assumed that the statistical segment length of PSS was identical to that of PS. The curve in Figure 8 through the data represents the least-squares RPA fit (eq 4) with $\chi_{\text{PSS-PMB}}$ as the adjustable parameter. The calculated $\chi_{\text{PSS-PMB}}$ of P1(31) is 0.329, which is located between $\chi_{\text{PSS-PMB}} = 0.194$ from the Leibler theory and $\chi_{\text{PSS-PMB}} = 0.395$ from Fredrickson−Helfand theory.

In reality, the PSS chains are copolymers comprising randomly located sulfonated styrene (SS) and unsulfonated styrene (S) monomers. There are thus three kinds of monomeric interactions in our copolymers: SS/MB, S/MB, and SS/S. Random copolymer theory (RCT) of mixing[54,55] can be used to relate $\chi_{\text{PSS-PMB}}$ to these monomeric interactions.

$$\chi_{\text{PSS-PMB}} = p\chi_{\text{SS-MB}} + (1-p)\chi_{\text{S-MB}} - p(1-p)\chi_{\text{SS-S}} \quad (5)$$

where p is the volume fraction of sulfonated monomers in the PSS chain and χ_{ij} represents the interaction parameter between i and j repeating units. The domain spacing, d, of lamellar diblock copolymers in the strong segregation limit can be expressed by[56]

$$d = \left(\frac{12}{\pi^2}\right)^{1/3} \left(\frac{\gamma}{k_B T}\right)^{1/3} N^{2/3} a^{2/3} v^{1/3} \quad (6)$$

where γ and a are the interfacial tension between polymer pairs and the average statistical segment length (calculated with respect to a reference monomer volume = 0.1 nm^3). γ can be expressed using the strong segregation theory of Hefand and co-workers[57]

$$\gamma = k_B T \frac{a}{v} \sqrt{\frac{\chi}{6}} \quad (7)$$

By combining (5), (6) and (7)

$$d^3 = \frac{12a^3}{\sqrt{6}\pi^2} (p\chi_{\text{SS-MB}} + (1-p)\chi_{\text{S-MB}} - p(1-p)\chi_{\text{SS-S}})^{1/2} N^2 \quad (8)$$

Equation 8 implies that $\chi_{\text{S-MB}}$, $\chi_{\text{SS-MB}}$, and $\chi_{\text{SS-S}}$ can be estimated from a plot of d^3 versus N^2 at different p values.

In Figure 9a we plot d^3 versus N^2 obtained from the six different samples, P3(19), P4(24), P5(21), P9(19), P4(7), and P21(5), that formed LAM at 25 °C. It is clear that the plot of d^3 versus N^2 is approximately linear for a given value of SL. The slopes of the lines for SL = 22 ± 2% and SL = 6 ± 1% are 0.067 and 0.041 nm^3, respectively. Using eqs 6 and 7, we estimate $\chi_{\text{PSS-PMB}} = 0.734$ for SL = 22 mol % ($p = 0.27$) and $\chi_{\text{PSS-PMB}} = 0.276$ for SL = 6 mol % ($p = 0.08$). Using the literature value of $\chi_{\text{S-MB}} = 0.21$ at 25 °C from ref 24, $\chi_{\text{SS-MB}} = 6.54$ and $\chi_{\text{SS-S}} = 5.89$ were obtained. Literature values for $\chi_{\text{SS-S}}$ vary between 5.6 and 25.[25,58] The reference volume used for determining $\chi_{\text{SS-S}}$ was not specified in refs 25 and 58 and thus quantitative comparison between our results and those in refs 25 and 58 cannot be made. To our knowledge, there are no previous measurements of $\chi_{\text{SS-MB}}$. Equation 5 then enables the determination of $\chi_{\text{PSS-PMB}}$ as a function of p at 25 °C. The dependence of $\chi_{\text{PSS-PMB}}$ on p thus obtained is shown by the curve in Figure 9b. It is clear that $\chi_{\text{PSS-PMB}}$ determined by RCT increases with increasing sulfonation. The $\chi_{\text{PSS-PMB}}$ parameters

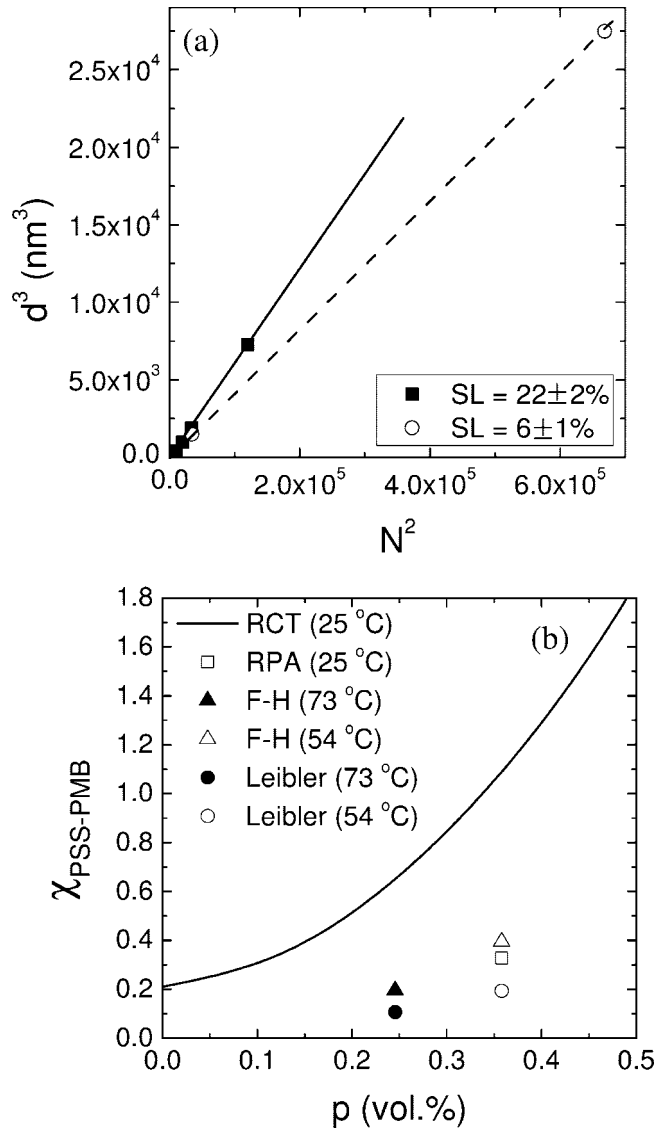

Figure 9. (a) Dependence of lamellar domain spacing (d) on chain length (N) for SL = 22 ± 2% and SL = 6 ± 1% shown in the format d^3 versus N^2. (b) Curve shows $\chi_{\text{PSS-PMB}}$ at 25 °C as a function of the volume fraction of sulfonated monomers in the PSS chain, p, calculated by random copolymer theory (RCT). Estimates of $\chi_{\text{PSS-PMB}}$ based on the RPA fit and ODT determinations are shown by symbols as indicated.

determined from the ODT measurements, shown by the triangles and circles in Figure 9b, also increase with increasing p. There is good agreement between $\chi_{\text{PSS-PMB}}$ determined by ODT measurements with that obtained by the RPA fit (square in Figure 9b). However, the $\chi_{\text{PSS-PMB}}$ values obtained by RCT are larger than those obtained from ODT measurements as shown in Figure 9b. It should be noted that eq 5 is a crude approximation, based on the concept of random mixing. Even in the case of model saturated hydrocarbon polymers, χ parameters based on RCT differ from measured χ parameters by factors as large as 3.[59] We therefore expect eq 5 to only provide a qualitative basis for interpreting the $\chi_{\text{PSS-PMB}}$ values shown in Figure 9b. The experimental uncertainties in the parameters such as a and N may also contribute to the differences in the χ parameters shown in Figure 9b.

Conclusion

The phase diagrams of symmetric PSS-PMB copolymers were mapped out as a function of molecular weight, SL, and temperature. Ordered LAM, gyroid, HPL, and HEX phases

were observed in spite of the fact that the PSS volume fraction lies between 0.45 and 0.50. In this range of compositions, only LAM phases are seen in conventional block copolymers. Due to the large value of χ between the sulfonated and non-sulfonated blocks, ordered nanostructures were observed in very low molecular weight block copolymers. For example, PSS-PMB (1.8K–1.4K) with 32% SL shows gyroid structure with 5 nm periodicity and PSS-PMB (3.0K–2.6K) with 19% SL forms lamellar structure with 7.5 nm periodicity. The low molecular weight samples show gyroid-to-disorder and lamellae-to-disorder phase transitions with increasing temperature. In contrast, the phase behavior of high molecular weight PSS-PMB copolymers (>7.7 kg/mol) is independent of temperature. These observations were combined with Leibler and Fredrickson−Helfand theories to provide estimates of $\chi_{PSS\text{-}PMB}$. Additional estimates of $\chi_{PSS\text{-}PMB}$ were obtained from SANS profiles measured from a disordered sample and a combination of the dependence of d on N and random copolymer theory. These measurements suggest that standard theories such as the random phase approximation and Flory–Huggins theory can be used to understand the molecular underpinnings of the observed order–disorder transitions. These theories, however, do not provide any insight into the origin of the complex ordered phases that we have observed in symmetric PSS-PMB copolymers.

Acknowledgment. Major funding for this work was provided through the Electron Microscopy of Soft Matter Program at Lawrence Berkeley National Laboratory (LBNL) supported by the Director, Office of Science, Office of Basic Energy Sciences, Materials Sciences and Engineering Division, of the U.S. Department of Energy under Contract No. DE-AC02-05CH11231. TEM was performed at the National Center for Electron Microscopy at LBNL. SAXS measurements were conducted at the Advanced Photon Source (APS) supported by the U.S. Department of Energy, Office of Science, Office of Basic Energy Sciences, under Contract No. DE-AC02-06CH11357, on the ChemMatCARS Sector 15 instrument which is principally supported by the National Science Foundation/Department of Energy under grant No. CHE-0535644. The SANS facilities at NIST are supported in part by the National Science Foundation under Agreement No. DMR-0504122.

References and Notes

(1) Leibler, L. *Macromolecules* **1980**, *13*, 1602.
(2) Fredrickson, G. H.; Helfand, E. *J. Chem. Phys.* **1987**, *87*, 697.
(3) Bates, F. S.; Fredrickson, G. H. *Annu. Rev. Phys. Chem.* **1990**, *41*, 525
(4) Matsen, M. W.; Bates, F. S. *Macromolecules* **1996**, *29*, 1091.
(5) Matsen, M. W.; Bates, F. S. *J. Chem. Phys.* **1997**, *106*, 2436.
(6) Cochran, E. W.; Garcia-Cervera, C. J.; Fredrickson, G. H. *Macromolecules* **2006**, *39*, 2449.
(7) Floudas, G.; Ulrich, R.; Wiesner, U. *J. Chem. Phys.* **1999**, *110*, 652.
(8) Qi, S.; Chakraborty, A. K.; Wang, H.; Lefebvre, A. A.; Balsara, N. P.; Shaknovich, E. I.; Xenidou, M.; Hadjichristidis, N. *Phys. Rev. Lett.* **1999**, *82*, 2896.
(9) Qi, S.; Chakraborty, A. *J. Chem. Phys.* **2000**, *112*, 1585.
(10) Qi, S.; Chakraborty, A.; Balsara, N. P. *J. Chem. Phys.* **2001**, *115*, 3387.
(11) Floudas, G.; Vazaiou, B.; Schipper, F.; Ulrich, R.; Wiesner, U.; Iatrou, H.; Hadjichristidis, N. *Macromolecules* **2001**, *34*, 2947.
(12) Elabd, Y. A.; Napadensky, E.; Walker, C. W.; Winey, K. I. *Macromolecules* **2006**, *39*, 399.
(13) Elabd, Y. A.; Beyer, F. L.; Walker, C. W. *J. Membr. Sci.* **2004**, *231*, 181.
(14) Soo, P. P.; Huang, B. Y.; Jang, Y. I.; Chiang, Y. M.; Sadoway, D. R.; Mayes, A. M. *J. Electrochem. Soc.* **1999**, *146*, 32.
(15) Trapa, P. E.; Huang, B. Y.; Won, Y. Y.; Sadoway, D. R.; Mayes, A. M. *Electrochem. Solid State* **2002**, *5*, A85.
(16) Singh, M.; Odusanya, O.; Wilmes, G. M.; Eitouni, H. B.; Gomez, E. D.; Patel, A. J.; Chen, V. L.; Park, M. J.; Fragouli, P.; Iatrou, H.; Hadjichristidis, N.; Cookson, D.; Balsara, N. P. *Macromolecules* **2007**, *40*, 4578.
(17) Lyklema, J. *Fundamentals of Interface and Colloid Science*; Academic Press: New York, 1995; Vol. *II*.
(18) Kimishima, K.; Jinnai, H.; Hashimoto, T. *Macromolecules* **1999**, *32*, 2585.
(19) Loo, Y.-L.; Register, R. A.; Adamson, D. H.; Ryan, A. J. *Macromolecules* **2005**, *38*, 4947.
(20) Won, J.; Park, H. H.; Kim, Y. J.; Choi, S. W.; Ha, H. Y.; Oh, I.-H.; Kim, H. S.; Kang, Y. S.; Jin, K. J. *Macromolecules* **2003**, *36*, 3228.
(21) Shi, Z.; Holdcroft, S. *Macromolecules* **2005**, *38*, 4193.
(22) Kim, J.; Kim, B.; Jung, B. *J. Membr. Sci.* **2002**, *207*, 129.
(23) Balsara, N. P.; Lin, C. C.; Dai, H. J.; Krishnamoorti, R. *Macromolecules* **1994**, *27*, 1216.
(24) Adams, J. L.; Quiram, D. J.; Graessley, W. W.; Register, R. A.; Marchand, G. R. *Macromolecules* **1998**, *31*, 201.
(25) Beck Tan, N. C.; Liu, X.; Briber, R. M.; Peiffer, D. G. *Polymer* **1995**, *36*, 1969.
(26) Brandrup, J., Immergut, E. H., Eds.; *Polymer Handbook*, 3rd ed.; John Wiley & Sons: New York, 1989.
(27) DeLongchamp, D. M.; Vogt, B. D.; Brooks, C. M.; Kano, K.; Obrzut, J.; Richter, C. A.; Kirillov, O. A.; Lin, E. K. *Langmuir* **2005**, *21*, 11480.
(28) Hajduk, D. A.; Gruner, S. M.; Rangarajan, P.; Register, R. A.; Fetters, L. J.; Honeker, C.; Albalak, R. J.; Thomas, E. L. *Macromolecules* **1994**, *27*, 490.
(29) Hajduk, D. A.; Ho, R.-M.; Hillmyer, M. A.; Bates, F. S.; Almdal, K. *J. Phys. Chem. B* **1998**, *102*, 1356.
(30) Benedicto, A. D.; OBrien, D. F. *Macromolecules* **1997**, *30*, 3395.
(31) Zhu, L.; Huang, P.; Chen, W. Y.; Cheng, S. Z. D.; Ge, Q.; Qurik, R. P.; Senador, T.; Shaw, M. T.; Thomas, E. L.; Lotz, B.; Hsiao, B. S.; Yeh, F.; Liu, L. *Macromolecules* **2003**, *36*, 3180.
(32) Khandpur, A. K.; Förster, S.; Bates, F. S.; Hamley, I. W.; Ryan, A. J.; Bras, W.; Almdal, K.; Mortensen, K. *Macromolecules* **1995**, *28*, 8796.
(33) Schulz, M. F.; Khandpur, A. K.; Bates, F. S.; Almdal, K.; Mortensen, K.; Hajduk, D. A.; Gruner, S. M. *Macromolecules* **1996**, *29*, 2857.
(34) Hajduk, D. A.; Takenouchi, H.; Hillmyer, M. A.; Bates, F. S.; Vigild, M. E.; Almdal, K. *Macromolecules* **1997**, *30*, 3788.
(35) Huggins, M. L. *J. Chem. Phys.* **1941**, *9*, 440.
(36) Flory, P. In *Principles of Polymer Chemistry*; Cornell University Press: Ithaca, NY, 1953; Chapter XIII.
(37) Mani, S.; Weiss, R. A.; Cantino, M. E.; Khairallah, L. H.; Hahn, S. F.; Williams, C. E. *Eur. Polym. J.* **2000**, *36*, 215.
(38) Semenov, A. N.; Anastasiadis, S. H.; Boudenne, N.; Fytas, G.; Xenidou, M.; Hadjichristidis, N. *Macromolecules* **1997**, *30*, 6280.
(39) Colby, R. H. *Curr. Opin. Colloid Interface Sci.* **1996**, *1*, 454.
(40) Fredrickson, G. H.; Bates, F. S. *Annu. Rev. Phys. Chem.* **1996**, *26*, 501.
(41) Park, S.; Cho, D.; Ryu, J.; Kwon, K.; Lee, W.; Chang, T. *Macromolecules* **2002**, *35*, 5974.
(42) Hajduk, D. A.; Gruner, S. M.; Rangarajan, P.; Register, R. A.; Fetters, L. J.; Honeker, C.; Albalak, R. J.; Thomas, E. L. *Macromolecules* **1994**, *27*, 490.
(43) Sakurai, S.; Momii, T.; Taie, K.; Shibayama, M.; Nomura, S.; Hashimoto, T. *Macromolecules* **1993**, *26*, 485.
(44) Ryu, C. Y.; Vigild, M. E.; Lodge, T. P. *Phys. Rev. Lett.* **1998**, *81*, 5354.
(45) Koga, T.; Hashimoto, T. *J. Chem. Phys.* **1999**, *110*, 11076.
(46) Jeong, U.; Lee, H. H.; Yang, H.; Kim, J. K.; Okamoto, S.; Aida, S.; Sakurai, S. *Macromolecules* **2003**, *36*, 1685.
(47) Rosedale, J. H.; Bates, F. S.; Almdal, K.; Mortensen, K.; Wignall, G. D. *Macromolecules* **1995**, *28*, 1429.
(48) Park, M. J.; Downing, K. H.; Jackson, A.; Gomez, E. D.; Minor, A. M.; Cookson, D.; Weber, A. Z.; Balsara, N. P. *Nano Lett* **2007**, *7*, 3547.
(49) Park, M. J.; Nedoma, A.; Geissler, P. L.; Balsara, N. P.; Jackson, A.; Cookson, D. *Macromolecules* **2008**, *41*, 2271.
(50) Balsara, N. P.; Jonnalagadda, S. V.; Lin, C. C.; Han, C. C.; Krishnamoorti, R. *J. Chem. Phys.* **1993**, *99*, 10011.
(51) Lin, C. C.; Jeon, H. S.; Balsara, N. P.; Hammouda, B *J. Chem. Phys.* **1995**, *103*, 1957.
(52) Bates, F. S.; Maurer, W. W.; Lipic, P. M.; Hillmyer, M. A.; Almdal, K.; Mortensen, K.; Fredrickson, G. H.; Lodge, T. P. *Phys. Rev. Lett.* **1997**, *79*, 849.
(53) Balsara, N. P.; Eitouni, H. *Physical Properties of Polymers Handbook*; Mark, J. E., Ed.; Springer: New York, 2007; Chapter 19.
(54) Krishnamoorti, R.; Graessley, W. W.; Balsara, N. P.; Lohse, D. J. *Macromolecules* **1994**, *27*, 3073.
(55) Graessley, W. W.; Krishnamoorti, R.; Balsara, N. P.; Fetters, L. J.; Lohse, D. J.; Schulz, D. N.; Sissano, J. A.; Butera, R. J.*Macromolecules* **1994**, *27*, 3896.
(56) Wang, Z.-G. *J. Chem. Phys.* **1994**, *3*, 2298.
(57) Helfand, E.; Sapse, A. M. *J. Chem. Phys.* **1975**, *62*, 1327.

(58) Zhou, N. C.; Xu, C.; Burghardt, W. R.; Composto, R. J.; Winey, K. I. *Macromolecules* **2006**, *39*, 2373.
(59) Krishnamoorti, R.; Graessley, W. W.; Balsara, N. P.; Lohse, D. J. *Macromolecules* **1994**, *27*, 3073.
(60) Disclaimer: Certain commercial equipment, instruments, or materials (or suppliers, or software) are identified in this paper to foster understanding. Such identification does not imply recommendation or endorsement by the National Institute of Standards and Technology, nor does it imply that the materials or equipment identified are necessarily the best available for the purpose.

MA702733F